22nd IAEA Fusion Energy Conference
Geneva, Switzerland Oct. 13-18, 2008

COMPARISON OF SMALL ELM CHARACTERISTICS AND REGIMES IN ALCATOR C-MOD, MAST, AND NSTX

R. Maingi[1], A.E. Hubbard[2], H. Meyer[3], J.W Hughes[2], A. Kirk[3], R. Maqueda[4], J.L. Terry[2], and the Alcator C-Mod, MAST, and NSTX teams

1) Oak Ridge National Laboratory, Oak Ridge TN, 37831 USA
2) Massachusetts Institute of Technology, Cambridge MA 02139
3) UKAEA Culham, Culham, U.K
4) Nova Photonics, Princeton, NJ 08543

This page intentionally left blank

Comparison of Small ELM Characteristics and Regimes in Alcator C-Mod, MAST, and NSTX

R. Maingi[1], A.E. Hubbard[2], H. Meyer[3], J.W Hughes[2], A. Kirk[3], R. Maqueda[4], J.L. Terry[2] and the Alcator C-Mod, MAST, and NSTX teams
(email: rmaingi@pppl.gov)
[1] *Oak Ridge National Laboratory, Oak Ridge TN, 37831 USA*
[2] *Massachusetts Institute of Technology, Cambridge MA 02139*
[3] *UKAEA Culham, Culham, U.K*
[4] *Nova Photonics, Princeton, NJ 08543*

Abstract. We report on the status of a set of ITPA-sponsored experiments among the Alcator C-Mod, MAST and NSTX devices to compare the characteristics and access conditions of small edge-localized modes (ELMs). Small ELM discharges were developed in each of the machines, and common features were identified, both in terms of ELM structure and operational windows. A common observation is an apparent β_{ped} threshold for small ELM access, although the absolute threshold value varied widely between the devices. In addition, most of the small ELM types had multiple filaments with propagation in the co-I_p direction.

I. Introduction

Periodic eruptions from the plasma periphery have been observed since the discovery of the high-confinement mode (H-mode) regime in tokamaks[1]. These ejections are termed edge localized modes (ELMs)[2], and one measure of the severity of ELMs is the fractional stored energy loss, $\Delta W_{tot}/W_{tot}$ where W_{tot} is the total plasma stored energy prior to the ELM. While the best plasma energy confinement is often correlated with large (Type I) ELMs with $\Delta W_{tot}/W_{tot}$ up to 0.2 per ELM, such large transient heat pulses are usually exhausted to the divertor targets, leading to erosion and target lifetime reduction[3]. Thus small ELM scenarios, i.e. with $\Delta W_{tot}/W_{tot} \leq 0.02$ per ELM, have been studied in many tokamaks and have commanded broad community interest[4-10], particularly those small ELM regimes with good energy confinement.

The urgency for development of small and no ELM scenarios has increased with the recent revision of the allowable ELM size in ITER to 1 MJ, representing about 0.3% of the 350 MJ plasma stored energy. Two approaches to actively mitigate large Type I ELMs being tested in the community include the use of Resonant Magnetic Perturbations (RMP)[11] and pellet pace-making[12]. In addition assessment of the applicability of the many naturally occurring

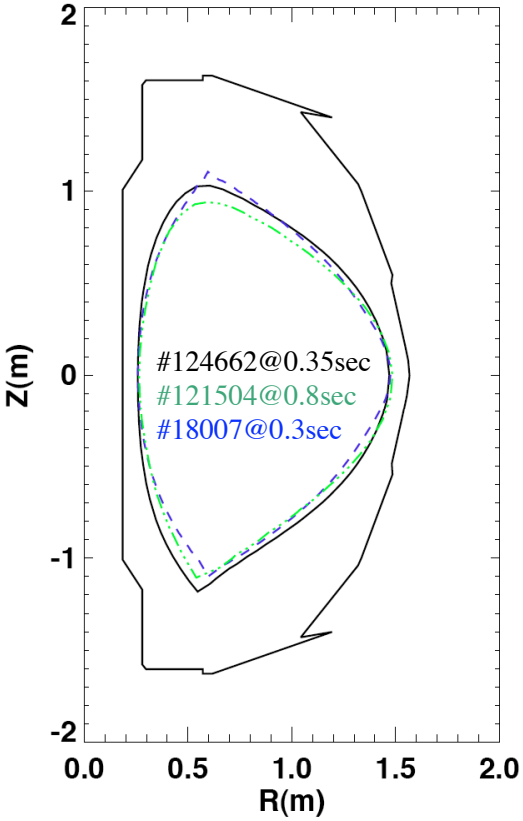

Fig. 1. Common shape developed for experiment. Color code: NSTX (black), MAST (blue: dashed), and C-Mod (green: dash-dot). The NSTX and C-Mod plots are scaled by 0.96 and 2.8 respectively, and the C-Mod boundary is shifted inward by 0.19 m.

small ELM regimes to ITER is the subject of ongoing research[13]. While these assessments have historically been made by examining the operational spaces of small ELM regimes in multiple devices, recent advances in diagnostic techniques now enable comparison of the ELM filamentary structure, which should provide additional insight into the underlying instabilities and improved physics-based extrapolability. In this paper, we present the first comparison of small ELM regimes in the Alcator C-Mod, MAST and NSTX devices, both in terms of operational windows and diagnostic signatures.

In Alcator C-Mod, the Enhanced D_α (EDA) regime[14, 15] is a high recycling regime without individual ELMs. A quasi-coherent edge oscillation is responsible for continuous density and impurity transport, preventing radiated power buildup typical of ELM-free H-modes[16]. The EDA H-mode has been shown[17] to evolve into a regime with individual small ELMs at sufficiently high pedestal temperature and/or pedestal β. Large, Type I ELMs have only been observed in shapes with large lower triangularity and small upper triangularity[18]. Type III ELMs, which are not studied in this paper, occur with low input power or high radiation, and are characterized by low edge electron temperature[19]. In MAST Type III ELMs (which are of intermediate size with $\Delta W_{tot}/W_{tot} \sim$ 1-3%) are usually observed[20], although Type I ELMs are also seen at the higher heating power levels. Small ELMs, which differ from both Type I and Type III ELMs, have been observed in specific circumstances, described in detail below. Finally in NSTX a wide range of ELMs including Type I and Type III ELMs has been observed. In addition, a small ELM regime, termed Type V ELMs, has been shown to have a wide operating window with unique low-n filamentary ELM structure[21]. In the remainder of this paper, we compare the characteristics of these small ELM regimes in all three devices, with the ultimate goal of determining if the underlying instability is the same in all three cases.

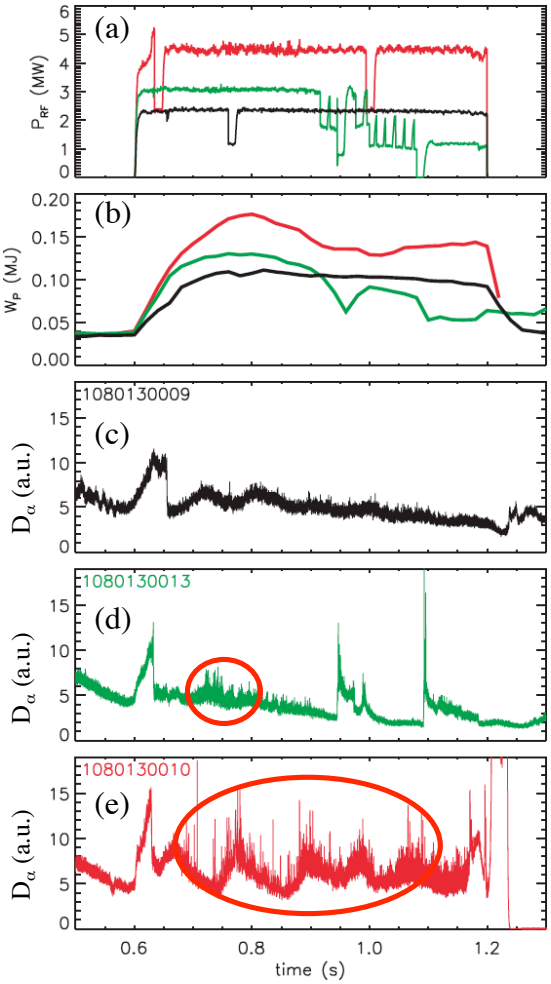

Fig. 2. ICRF heating power scan in Alcator C-Mod with (a) ICRF power, (b) plasma stored energy, and (c)-(e) D_α emission from each discharge. Small ELMs are present in panels (d) and (e).

II. Summary of experiments

A true dimensionless comparison matching plasma boundary shape, normalized gyro-radius (ρ*), normalized collisionality (ν*), and normalized plasma pressure (β) is not possible because C-Mod, as a conventional tokamak, has a minimum aspect ratio R/a ~ 2.7, as compared with the typical aspect ratio range ~ 1.3-1.5 for the MAST and NSTX spherical

tokamaks. In addition the typical C-Mod pedestal β is ~10% of the MAST and NSTX values, owing partly to the order of magnitude difference in toroidal field, B_t, preventing an overlap in that quantity. On the other hand, poloidal β can be comparable between these devices. Thus, it was decided to match the scaled poloidal cross-sections in the three devices (e.g. Figure 1), while trying to also match the edge safety factor q95. The latter was chosen in part because q95 was observed[22] to be a critical parameter in establishing the similarity between EDA H-mode in C-Mod and the High Recycling Steady (HRS) H-mode[23] in JFT-2M. A heating power scan in each device then provided an electron collisionality ν_e^* and normalized pedestal pressure β_{ped} scan for determination of the small ELM de-stabilization threshold conditions.

IIa. Alcator C-Mod results

In the Alcator C-Mod device, the small ELM regime was observed in a lower-single null boundary shape with plasma current I_p=0.8 MA, B_t=5.2 T, q95=5.5, elongation κ=1.7, lower triangularity δ_L=0.5, and magnetic balance parameter δ_r^{sep} ~ -5mm (defined as the radial distance between the two X-point flux surfaces mapped to the outer midplane). Figure 2 shows the D_α traces for the discharges in a power scan, in which small ELMs are observed (red ovals). An apparent rf power threshold of ~ 3 MW is required to access small ELMs, consistent with thresholds in normalized plasma pressure (*i.e.*, β_N>1.3) previously observed at higher power in more typical C-Mod equilibria[17]. The threshold value for β_{ped} was ~ 0.3%, where $\beta_{ped}=4\mu_0 P_e^{ped}/|B_{ped}|^2$, μ_0 is the permeability of free space, and $|B_{ped}|$ is the magnitude of the total magnetic field at the outer midplane pedestal. The small ELMs were still present at the highest rf power level of 4.5 MW (β_{ped} > 0.5%). The ν_e^* range (assuming Z_{eff}=1 here and for other devices) at the top of the pedestal was between 0.5 and 4 for these discharges. The I_p window in the shape used for these experiments appears to be narrow in that changes of +/- 50 kA eliminated all signs of small ELMs. In addition, the δ_r^{sep} could be changed only by +/- 1-2mm before access to the small ELM regime was lost. The operational window in δ is at least 0.50+/- 0.02. Note that the large ELMs in C-Mod are seen in the high δ_L ~ 0.75 JFT-2M shape[18] (with δ_U ~ 0.15). The small ELMs were visible on the edge soft X-ray emission, fast magnetics, and gas puff imaging (GPI) diagnostic[24], although their individual impact on stored energy is indiscernible from the statistical noise on equilibrium reconstructions.

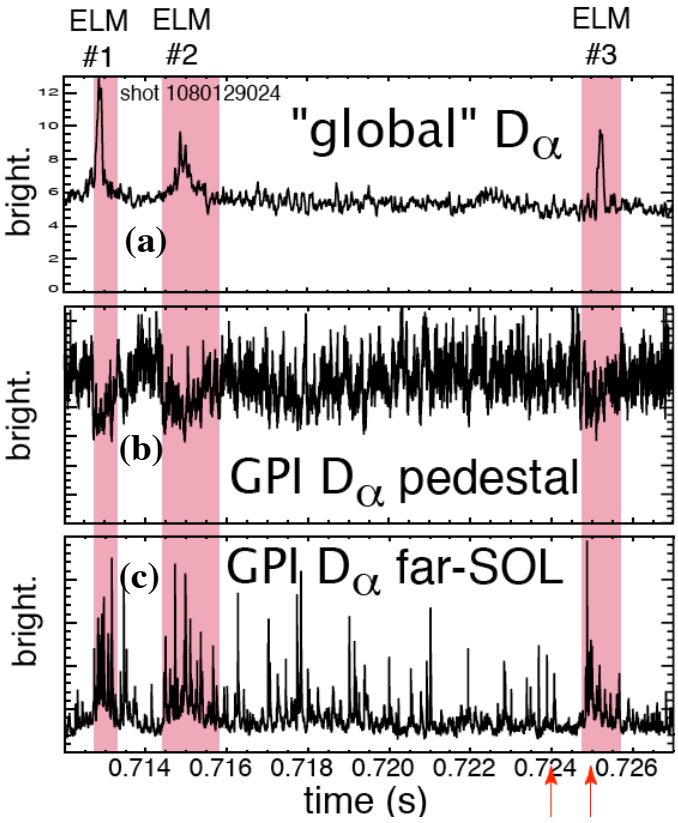

Fig. 3. C-Mod data from (a) a global D_α signal (b) a D_α signal near the top of the pedestal, and (c) a D_α signal in the far SOL. Panels (b) and (c) are from the GPI diagnostic.

While the small ELMs have similar appearance to the turbulence filaments in the raw

GPI data, subtle differences can be observed. Figure 3 shows three small ELMs in the shaded regions (panel (a)), along with GPI D_α emission from the pedestal (panel (b)) and far SOL regions (panel (c)). While individual filaments can be seen in panel (c), the small ELMs appear as bursts of filaments that are accompanied by a decrease in the pedestal D_α emission (panel (b)). In addition, the movement of the ELM filaments is mainly radial with possibly a slight downward component, i.e. which would be consistent with the ion diamagnetic drift direction or co-I_p direction, and in the dominant direction as the turbulence filaments.

IIb. MAST results

In the MAST device, small ELMs have been obtained in double-null boundary shapes with I_p=0.7 MA, B_t=0.5 T, q95=5.5, κ=1.9, δ=0.43, δ_r^{sep} ~ 0 mm. A power scan was conducted to determine the operational window for small ELMs. Figure 4 displays the discharges from the power scan, along with plasma stored energy and D_α emission. Type III ELMs were observed in panels 4c-4f and the early time of 4g; large Type I ELMs can be seen at the later times in panel 4g. The small ELMs are best seen as the small oscillations in panel 4f between 0.29-0.33 sec. (red oval). However careful inspection of the data showed that they were present between the Type III ELMs in panels 4c-4e also, but clearly absent when Type I ELMs appear in 4g. In terms of collisionality, the small ELMs occurred over a wide range: 1.5

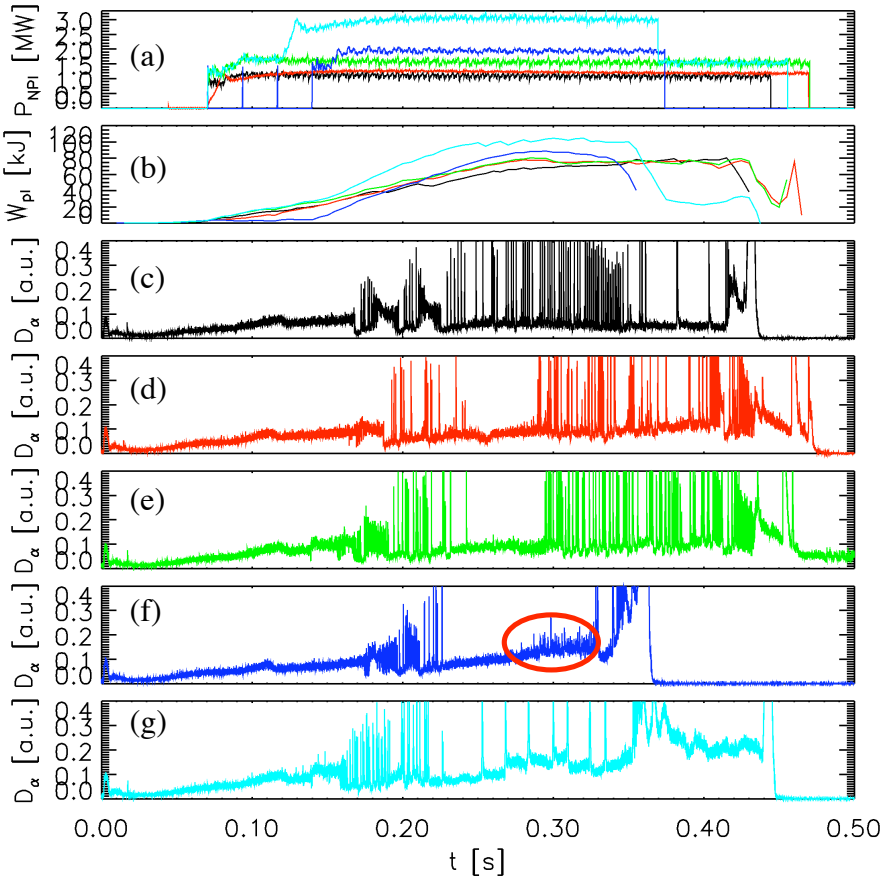

Fig. 4. Characteristics of MAST discharges with an NBI power scan. The NBI power is shown in panel (a), and plasma stored energy in panel (b), and the divertor D_α characteristics of each discharges in the NBI scans in panels (c)-(g).

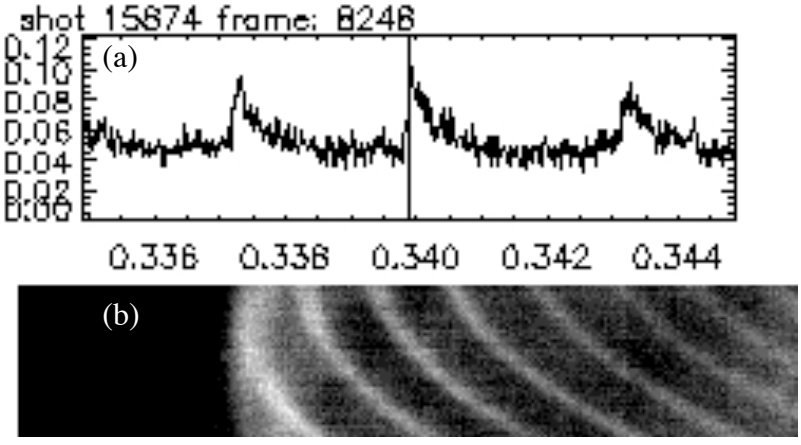

Fig. 5. MAST data: (a) D_α trace during small ELMs, and (b) portion of wide angle view of plasma, showing a large number of discrete filaments.

$< \nu_e^* < 20$, inter-mixed with Type III ELMs in the upper range while completely disappearing at the lower range as Type I ELMs appeared. We note that it was not possible to obtain H-mode with $\delta_r^{sep} < -0.6$ cm in these particular plasmas, consistent with previous observations of reduced power threshold in a double-null shape[25]. In smaller lower-single null shapes with reduced δ_U and $\delta_r^{sep} < -4$ cm H-mode is readily achieved, but no small ELMs have been observed so far.

The small ELMs have a high-n structure, with more filaments than the 10-20 typically observed[26] during Type I ELMs. Figure 5 shows the visible light from a portion of a wide-angle camera view of the MAST plasma. A regular banded, filamentary structure is observed in panel 5b during the ELM growth in panel 5a. The filament propagation is consistent with the toroidal rotation of the pedestal (or the ion diamagnetic drift direction as long as the filaments are attached to the plasma). This is similar to the inter-ELM turbulence filaments on MAST and C-Mod. The dynamics of these small ELMs differ from large ELMs[27, 28] and inter-ELM filaments on MAST in that most of the filaments from these ELMs do not detach from the plasma, i.e. they do not accelerate radially toward the outer wall.

IIc. NSTX results

In the NSTX device, two distinct classes of small ELMs have been identified. In near double-null boundary shapes that slightly favor the lower divertor and are otherwise similar to the MAST device shapes (I_p=0.9 MA, B_t=0.42 T, q95=5.5, κ=1.8, δ=0.5, -2mm $< \delta_r^{sep} <$ -6mm), an intermediate-n small ELM has been identified in a narrow heating power window. We tentatively refer to this ELM as Type II, owing to its appearance in near double-null shape[5]. Panel 6d shows the occurrence of this Type II ELM regime with a red oval; Type III ELMs are apparent in panel 6e and Type I ELMs are the large perturbations in panels 6c-6d. In discharges that more strongly favor the lower divertor ($\delta_r^{sep} \sim$ -15mm, reduced X-point height required for H-mode access), the more common type V ELM regime[29, 30] with single or double filaments in a broad β_{ped} window is recovered. At the highest heating power in panel 6g, Type I ELMs are inter-mixed with Type V ELMs. Note that H-mode access was not possible with q95=5.5 at large δ_r^{sep}; thus, the discharges in panels 6e-6i were obtained with q95 between 9-10. We also obtained an H-mode power scan with q95=8 in a different set of experiments, which confirmed that the type V ELM access window is independent of q95 as

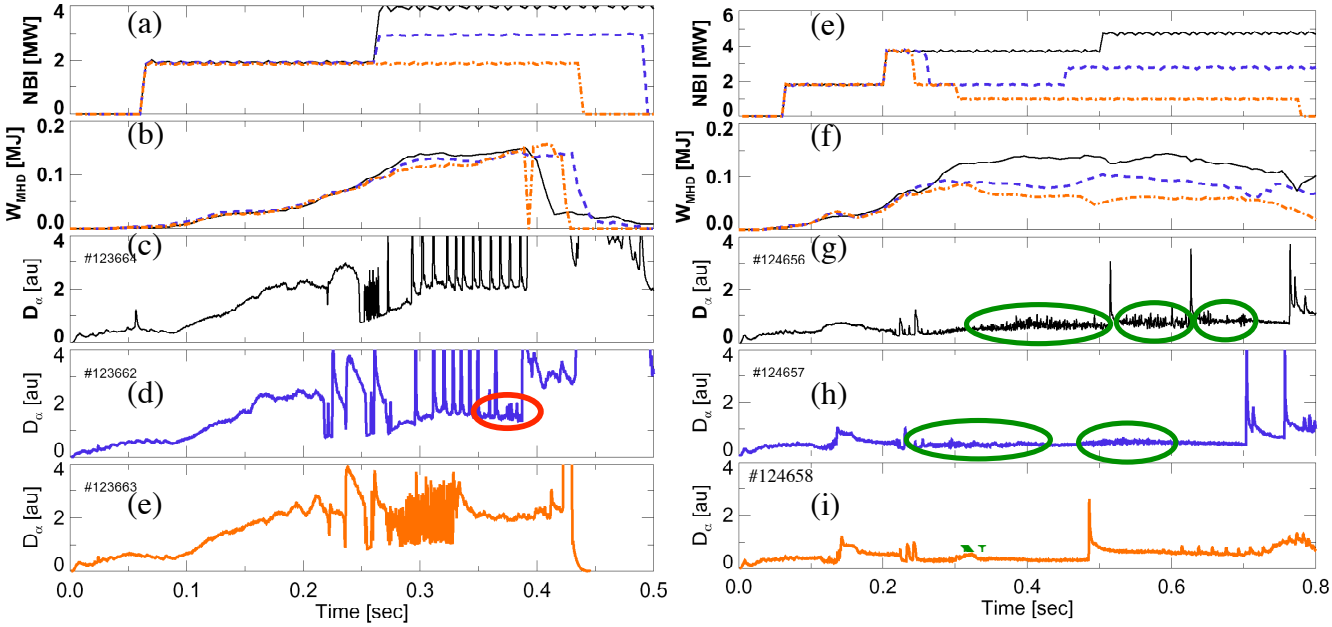

Fig. 6. Characteristics of NSTX discharges in power scan. The left panels (a)-(e) were taken with δ_r^{sep} = -0.6cm, whereas the right panels (e)-(i) were with δ_r^{sep}=-1.5cm and a lower X-point height. The red oval highlights small ELM in panel (d) and the green ovals Type V ELMs in panels g,h.

previously reported[31].

The differences in ELM structure between the Type II ELMs in panel 6d and Type V ELMs in panels 6g-6h are clearly shown in GPI data[32]. Specifically the field-aligned diagnostic views a gas puff near the plasma boundary to produce a 23cmx23cm radial (x-axis) and vertical (y-axis) cross section of the emission (Figure 7a). Figure 7b shows that the Type II ELM has multiple filaments in the GPI view, indicating a higher equivalent poloidal/toroidal mode number. The filaments clearly propagate downward poloidally, i.e. qualitatively consistent with the ion diamagnetic drift direction or the toroidal velocity of the pedestal as observed for the C-Mod and MAST small ELMs. In contrast, the Type V ELMs have a single/double filamentary structure as shown in Figure 7c, and clearly propagate upward, i.e. in the electron diamagnetic drift or counter-I_p direction. In addition, the type V ELM typically spawns secondary turbulence filaments[33], as shown in frames 39-80 in figure 7b. Note that the primary filament of the Type V ELM often does not detach from the plasma, as observed for the MAST small ELM. Neither of the small NSTX ELMs discussed here has a measurable impact on plasma stored energy, i.e. $\Delta W_{tot}/W_{tot} \leq 0.01$.

III. Discussion and summary

The edge n_e and T_e profiles from each device were fit with a modified tanh function to obtained pedestal values, from which pedestal β and ν_e^* were computed[25, 31, 34]. The data from the three devices is compared for the periods with and without small ELMs in Figure 8. The C-Mod data (triangles) show that the small ELMs are observed in the higher β_{ped} range of the data, with no apparent ν_e^* dependence. The MAST data (squares) show a broad β_{ped} range from 0.3-3%, with the small ELMs disappearing when $\beta_{ped} >$ 3% and when $\nu_e^* < 2$ (Type I ELMS appeared). The NSTX Type V ELM data show a somewhat higher threshold, i.e. $\beta_{ped} > 5\%$ is needed for access. The Type V ELMs are present even at the highest $\beta_{ped} \sim 20\%$, albeit between Type I ELMs.

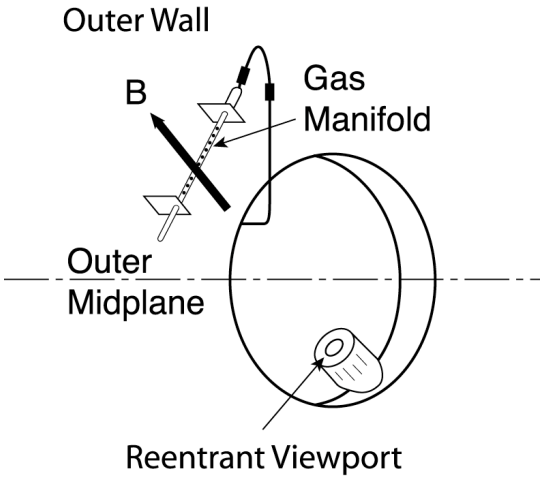

Fig. 7a. GPI setup on NSTX, showing camera view of gas manifold along B.

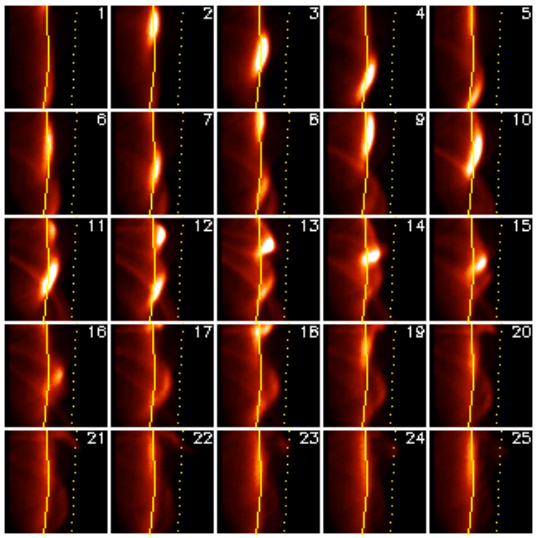

Fig. 7b. NSTX Type II ELM images with GPI from #123656, t=339.217, 8.1 μs per frame.

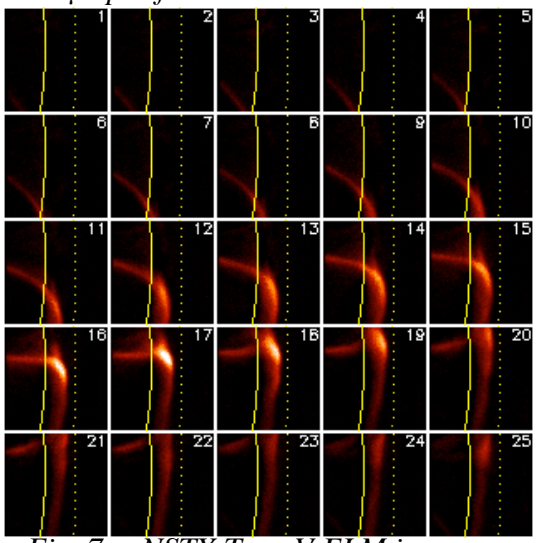

Fig. 7c. NSTX Type V ELM image with GPI from #119318, starting at t=668.277 at 8.1 μs per frame. The solid line represents the EFIT

Thus, one general feature of these small ELM scenarios is that access occurs in apparent β_{ped} windows, although the details differ between the devices. As mentioned above, because of the difference in aspect ratio, different definitions of beta (referenced to average or pedestal B) scale differently in these devices; the observed difference indicates that either that the β_{ped} definition used is not the controlling parameter for this instability, or that the threshold itself depends on R/a. There is, however, no consistent role of ν_e^*. The visible camera images of ELMs show some common features with inter-ELM turbulence filaments, but with important distinctions in each machine. In C-Mod, the small ELMs affect the emission in the pedestal and generate bursts of detached filaments. In MAST, the small ELMs have a periodic structure with more filaments than larger ELMs, and most of the filaments do not detach from the plasma. In both C-Mod and MAST, the propagation of the ELM filaments and turbulence filaments is consistent with the ion diamagnetic drift direction or the pedestal top toroidal rotation velocity. In NSTX, the Type V ELMs contain one or two filaments, but these propagate in the counter I_p direction consistent with electron diamagnetic drift direction, i.e. opposite to the Type II ELMs discussed above and normal turbulence filaments. Note that we omit plotting of the NSTX Type II ELM data for clarity because the access window is so narrow. For reference, the β_{ped} and ν_e^* ranges were between 6-9% and 0.8-2.2 respectively in the NSTX Type II ELM discharges. Thus we submit 1) that the Type V ELMs are indeed distinct from the C-Mod and MAST small ELMs, and 2) that the NSTX Type II ELMs have a poloidal propagation direction similar to the small ELMs on C-Mod and MAST.

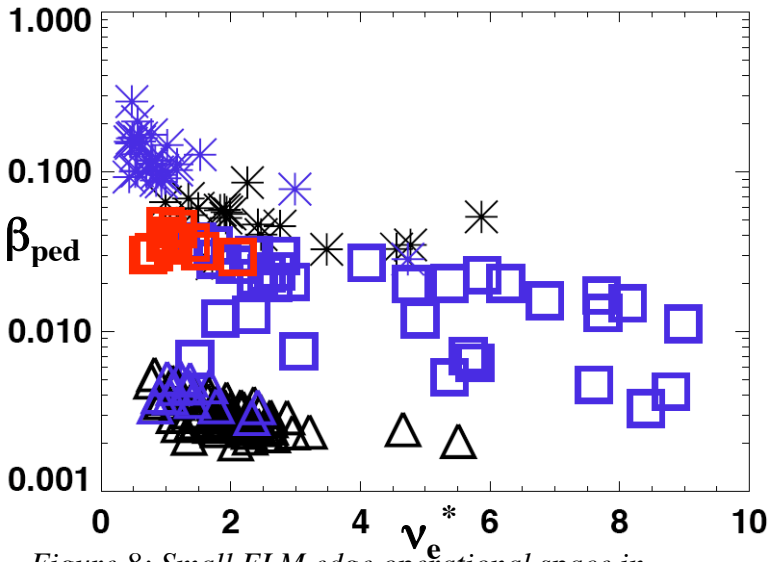

Figure 8: Small ELM edge operational space in Alcator C-Mod (triangles), MAST (squares), and NSTX (stars – Type V ELMs only). The color BLACK signifies no small ELMs, BLUE signifies that small ELMs were observed, and RED signifies that only large ELMs observed (no small ELMs mixed in). The C-Mod data are from EDA H-modes, the MAST data from small ELMs in double-null configuration, and the NSTX data from Type V ELMy H-mode.

One straightforward conclusion from these studies is that small ELMs can indeed have different toroidal mode structure and operational windows, even within a single device. Thus there may be multiple scenarios by which small ELMs could be achieved naturally in ITER. In addition, subtle changes in shape, particularly the magnetic balance as characterized by δ_r^{sep}, can modify access to these small ELM scenarios.

Stability analysis of these ELMs is complicated because the resulting profile relaxation is quite subtle, obviating stability comparisons based on the "before" and "after" ELM profiles. Ideal MHD calculations of the NSTX discharges with Type V ELMs previously indicated stability to low-n and high-n ideal modes, possibly pointing to the need for resistive MHD calculations, which are commencing. Ideal MHD calculations for C-Mod and MAST are commencing, and will help identify whether the small ELMs are, as in previous C-Mod experiments, at the peeling ballooning boundary as expected for Type II ELMs.

III. Acknowledgements

This research was supported in part by the U.S. Dept. of Energy Contracts DE-AC05-00OR22725, DE-FC02-99ER54512, DE-FG02-04ER54767, and DE-AC02-76CH03073, and the U.K. Engineering and Physical Sciences Research Council. We gratefully acknowledge the contribution of the technical and operations staff from Alcator C-Mod, MAST, and NSTX. In addition, we acknowledge the valuable discussion and support from the ITPA pedestal physics working group.

References

[1] F. Wagner, et. al., *Physical Review Letters* **49** (1982) 1408.
[2] H. Zohm, et. al., *Plasma Physics Controlled Fusion* **36** (1994) A129.
[3] A. Loarte, et. al., *J. Nucl. Materials* **313-316** (2003) 962.
[4] T. Ozeki*, et al.*, et. al., *Nuclear Fusion* **30** (1990) 1425.
[5] J. Stober, et. al., *Nuclear Fusion* **41** (2001) 1123.
[6] G. Saibene, et. al., *Nuclear Fusion* **45** (2005) 297.
[7] A. W. Leonard, et. al., *J. Nucl. Materials* **290-293** (2001) 1097.
[8] G. Saibene, et. al., *Plasma Physics Controlled Fusion* **44** (2002) 1769.
[9] Y. Kamada, et. al., *Plasma Physics Controlled Fusion* **42** (2000) A247.
[10] N. Oyama, et. al., *Nuclear Fusion* **45** (2005) 871.
[11] T. E. Evans, et. al., *Physical Review Letters* **92** (2004) 235003.
[12] P. T. Lang, et. al., *Nuclear Fusion* **45** (2005) 502.
[13] N. Oyama, et. al., *Plasma Physics Controlled Fusion* **48** (2006) A171.
[14] Y. Takase, et. al., *Physics of Plasmas* **4** (1997) 1647.
[15] M. Greenwald, et. al., *Phys. Plasma* **6** (1999) 1943.
[16] J. W. Hughes, et. al., *Fusion Science Techn.* **51** (2007) 317.
[17] D. A. Mossessian, et. al., *Physics of Plasmas* **10** (2003) 1720.
[18] J. L. Terry, et. al., *J. Nucl. Mater.* **363-365** (2007) 994.
[19] A. E. Hubbard, et. al., *Plasma Phys. Contr. Fusion* **5** (2005) 1744.
[20] A. Kirk, et. al., *Plasma Physics Controlled Fusion* **46** (2003) 551.
[21] R. Maingi, et. al., *Nuclear Fusion* **45** (2005) 264.
[22] A. E. Hubbard, et. al., *Plasma Phys. Contr. Fusion* **48** (2006) A121.
[23] K. Kamiya, et. al., *Plasma Physics Controlled Fusion* **46** (2004) A157.
[24] J. L. Terry, et. al., *Phys. Plasma* **10** (2003) 1739.
[25] H. Meyer, et. al., *Plasma Physics Controlled Fusion* **47** (2005) 843.
[26] A. Kirk, et. al., *Plasma Physics Controlled Fusion* **47** (2005) 993.
[27] A. Kirk, et. al., *Physical Review Letters* **92** (2004) 245002.
[28] A. Kirk, et. al., *Physical Review Letters* **96** (2006) 185001.
[29] R. Maingi, et. al., *Physics of Plasmas* **13** (2006) 092510.
[30] R. J. Maqueda, *et al.*, et. al., *J. Nucl. Materials* **363-365** (2007) 1000.
[31] R. Maingi, et. al., *Nuclear Fusion* **45** (2005) 1066.
[32] R. J. Maqueda, et. al., *Review of Scientific Instruments* **72** (2001) 931.
[33] R. J. Maqueda, et. al., *J. Nucl. Mater.* (2008) submitted.
[34] J. W. Hughes, et. al., *Phys. Plasma* **13** (2006) 056103.